Original Article

Acute hypoxia induces apoptosis in serum-deprived prostate cancer LNCaP cells

Weiyong Liu[1], Yunkai Zhu[1], Jun Jiang[1], Xuechao Jiang[2], Yaqing Chen[1]

[1]Department of Ultrasound, [2]Scientific Research Center, Xinhua Hospital Affiliated to Shanghai Jiaotong University School of Medicine, Shanghai 200092, China

Contributions: (I) Conception and design: W Liu, Y Chen; (II) Administrative support: Y Chen; (III) Provision of study materials: Y Chen, Y Zhu, J Jiang, X Jiang; (IV) Collection and assembly of data: W Liu, Y Zhu, J Jiang, X Jiang; (V) Data analysis and interpretation: W Liu, J Jiang, Y Chen; (VI) Manuscript writing: All authors; (VII) Final approval of manuscript: All authors.

Correspondence to: Yaqing Chen, MD, PhD. Department of Ultrasound, Xinhua Hospital Affiliated to Shanghai Jiaotong University School of Medicine, 1665 Kongjiang Road, Shanghai 200092, China. Email: chenyaqing@xinhuamed.com.cn.

Background: Human prostate cancer LNCaP cells can develop an androgen-sensitive prostate cancer animal model that closely mimic clinical disease. However, implantation of LNCaP cells yields a low take rate when subcutaneously xenografted in immunodeficient mice. Given that LNCaP cells are sensitive to hypoxia, we hypothesized that LNCaP cells might undergo substantial apoptosis in response to acute hypoxia under conditions of serum deprivation.

Methods: Serum-deprived LNCaP cells were cultured and exposed to either normoxic (21.0% O_2) or hypoxic (1.0% O_2) conditions. Morphological changes in nuclei were evaluated with Hoechst 33258 staining under fluorescence microscopy. Cell viability and migration were assayed by Cell Counting Kit-8 (CCK-8) and wound healing assay, respectively. The production of intracellular reactive oxygen species (ROS) was measured by a fluorescent probe assay. Apoptosis, mitochondrial membrane potential ($\Delta\Psi m$), and the cell cycle of LNCaP cells were analyzed by flow cytometry.

Results: Serum-deprived LNCaP cells tended to form multicellular aggregates, and the viability and migration of LNCaP cells were markedly suppressed under acute hypoxia. Acute hypoxia exposure for 24 hours induced significant ROS production, which was distributed heterogeneously among cells. LNCaP cells exhibited a time-dependent increase in apoptosis under acute hypoxia by flow cytometric analysis. Furthermore, acute hypoxia induced the collapse of the $\Delta\Psi m$ of LNCaP cells, and it also increased cell cycle arrest at the G0/G1 phases in a time-dependent manner.

Conclusions: Acute hypoxia induces substantial apoptosis in LNCaP cells under conditions of serum deprivation. The findings may provide valuable information for improving the tumor-formation method of LNCaP subcutaneous xenografts in nude mice.

Keywords: Acute hypoxia; apoptosis; LNCaP; prostate cancer; serum deprivation.

Submitted May 24, 2017. Accepted for publication Sep 22, 2017.
doi: 10.21037/tcr.2017.10.13
View this article at: http://dx.doi.org/10.21037/tcr.2017.10.13

Introduction

Prostate cancer is the most commonly diagnosed malignancy and the second-leading cause of cancer-related deaths in the United States (1). In addition, recent data have shown that the standardized incidence and mortality rates of prostate cancer are increasing rapidly in China (2). Most prostate cancers are androgen-dependent at the time of diagnosis, and treatment for prostate cancer may involve surgery, radiation, and drugs. However, prostate cancer cells become resistance to anti-androgen therapy when they acquire an androgen-independent growth capacity (3), resulting in a poor prognosis of such patients. Thus, it

is necessary to explore novel curative strategies, such as cancer-targeting identification for drug discovery, to improve the survival rate of patients. In this process, animal models are pivotal to bridge the translational gap from the bench to the clinic (4).

LNCaP xenograft models can closely mimic the disease progression of prostate cancer in an androgen-dependent state (5). LNCaP subcutaneous implantation is convenient yet poorly tumorigenic (6). Although the take rate increases with the addition of Matrigel to the inoculated cells, a modest 50% success rate is far from satisfactory (7). Some factors affecting successful subcutaneous tumor engraftment include the inoculated cell density, mouse age, and mouse strain, which are under investigation (8). Recently, the subcutaneous microenvironment at the implantation site of nude mice has been identified as an underlying factor (9). The subcutaneous implantation along the back of male mice reflects a poor blood supply, an acute hypoxic microenvironment, and inferior cell survival (10). LNCaP cells have a higher rate of oxygen consumption compared with DU145 and PC3 cells (11). Thus, it is conceivable that acute hypoxia at the ischemic subcutaneous site may be a vital factor for a decreased LNCaP engraftment rate.

Hypoxia differentially influences the cell apoptosis of different cancer cell lines (12). In a variety of cell types, hypoxia may render certain types of tumor cells resistant to hypoxia-induced apoptosis though metabolic inhibition (13) or directly induce cellular apoptosis in other types of tumor cells (14). The molecular mechanisms underlying the selection of cells that become apoptotic or survive by adapting to hypoxia remain unknown. We thus designed serum-deprived, acute hypoxic conditions to explore the tumorigenic properties of LNCaP cells. The results will help us to better understand the role of acute hypoxia on the apoptotic properties of serum-deprived LNCaP cells, which may provide some helpful information in the improvement of LNCaP engraftment procedure in future experiments *in vivo*.

Methods

Cell culture and acute hypoxia treatment

LNCaP cells were cultured in Dulbecco's modified Eagle medium (DMEM)/F-12 Ham (Gibco/BRL, NY, USA) supplemented with 10% fetal bovine serum (Gibco, Australia) in a HERACELL 150i CO_2 incubator (Thermo Scientific, USA) at normoxic conditions (21.0% O_2, 5.0% CO_2, N_2 balance). When cells approached nearly 80% confluence, the cells were washed twice with phosphate-buffered saline (PBS), and the medium was replaced by serum-deprived DMEM/F12. Then, the cells were maintained at normoxic or exposed to hypoxic conditions. Hypoxic conditions were established by culturing LNCaP cells in a hypoxic chamber (HERACELL 150i CO_2 Incubator, Thermo Scientific, USA) filled with 1.0% O_2, 5.0% CO_2, and N_2 balance. Following treatment, all experiments were performed in triplicate at the time points of 12, 24, and 48 hours.

Morphological analysis and Hoechst 33258 staining

Cell morphology were observed by light microscopy using a Leica EC3 microscope (Wetzlar, Germany) at the indicated times. Morphological changes in nuclei were evaluated by fluorescence microscopy with the chromatin dye Hoechst 33258 (Beyotime, China). In brief, cells in a 6-well microtiter plate (Costar, Corning, NY, USA) were fixed in cold 4% paraformaldehyde for 10 min at room temperature. Then, the cells were washed twice with cold PBS and incubated with Hoechst 33258 for 5 min in the dark. Nuclear chromatin morphology was assessed using a Leica EC3 fluorescence microscope (Wetzlar, Germany) at 200× magnification.

Cell viability assay

LNCaP cells were seeded in 96-well plates (Costar, USA) at a density of 50,000 cells per well. After treatment, cells were washed twice with PBS and 100 µL of fresh culture medium containing 10 µL of CCK-8 (Beyotime, China) was added to each well for additional 2 hours incubation. Cell viability at 12, 24, and 48 hours was determined by reading the absorbance at 450 nm using a BioTek µQuant Microplate Reader (Biotek Instruments Inc., Winooski, VT, USA). The inhibition rate of cell growth was calculated by the following formula: inhibition rate (%) = (1– average absorbance of treated cells at the indicated time/average absorbance of the cells at 0 hour) ×100%.

Wound healing assay

The wound healing assay was performed to assess tumor cell migration, as described previously (15). Gap closure at the indicated time was monitored by light microscopy at a magnification of 40×. The area of wound closure was

analyzed by Image-Pro Plus software (Media Cybernetics, Silver Spring, MD, USA). Wound healing was quantified as the percentage of area reduction compared with the initial scratch area.

Measurement of reactive oxygen species (ROS) generation

Intracellular accumulation of ROS was measured by a 2',7'-dichlorofluorescein diacetate (DCFH-DA, Beyotime, China) fluorescent probe assay. After treatment, the medium in black 96-well assay plates was replaced with serum-deprived culture medium containing DCFH-DA (10 μM) at 37 ℃ for 20 min in the dark. The cells were washed with serum-free medium to remove the residual probes. The cellular mean fluorescence intensity (MFI) was read by a Synergy™ H4 Hybrid Microplate Reader (BioTek Instruments Inc., USA), with an excitation wavelength of 485 nm and an emission wavelength of 528 nm. Gen5 software (BioTek Instruments Inc., USA) was used to measure the fluorescence data.

Dichlorofluorescein (DCF)-induced cytosolic fluorescence intensity analysis

Fluorescence images of cells were observed and photographed using the Leica EC3 inverted fluorescence microscope (Wetzlar, Germany). DCF-induced integrated mean fluorescence intensity (iMFI) within individual cells was measured using Image J software version 1.42q (NIH, Bethesda, MD, USA). The iMFI values were calculated following delineation of each cell and correction for the background.

Detection of apoptosis

The early apoptosis or late apoptosis/death of cells was evaluated by staining with an Apoptosis Detection Kit (Beyotime, China) following the manufacturer's instructions. Approximately 10,000 cells were analyzed in each sample. The floating and adherent cells were pooled together using trypsin (0.25%) ethylenediaminetetraacetate (EDTA) solution (Gibco, USA). After washing twice with cold PBS, the harvested cells were resuspended gently in 195 μL of annexin-binding buffer and stained with 5 μL of fluorescein isothiocyanate-conjugated annexin-V and propidium iodide (PI) solution. Cell were incubated for 20 min at room temperature in the dark, then analyzed with a FACS Canto™ II flow cytometer (BD Biosciences, San Jose, CA, USA) within 30 min. Data were examined using FlowJo software (version 7.6.1, Tree Star Inc., Ashland, OR, USA).

Detection of ΔΨm

The change of ΔΨm was determined using the JC-1 ΔΨm assay kit (Beyotime, China) on a FACS Canto™ II flow cytometer (BD Biosciences, USA). After exposure to either normoxic or hypoxic conditions, the cells were washed twice with PBS and stained with JC-1 working solution at 37 ℃ for 20 min. The stained cells were rinsed twice with cold JC-1 staining buffer. Then, the JC-1-stained cells were collected and illuminated using an excitation of 488 nm and collected with 530 nm bandpass emission filters. A dot plot was generated to track the fluorescence of polarized JC-1 aggregates (red) and depolarized JC-1 monomers (green).

Cell cycle analysis

For each sample, approximately 10,000 cells in a 6-cm culture dish were harvested by 0.25% trypsin solution. After washing twice with ice-cold PBS, the cells were collected and fixed using 70% ice-cold ethanol at –20 ℃ for at least 3 hours. Then, the cells were incubated in 500 μL of PI/RNase A staining buffer (Beyotime, China) for 30 min at room temperature in the dark. After filtering through a 70-μm nylon mesh, the stained cells were analyzed on BD FACS Canto II flow cytometer. The percentages of apoptosis-, G0/G1-, S-, and G2/M-phase cells were analyzed by a ModFit LT software package (Becton Dickinson, San Jose, CA, USA).

Statistical analysis

The SPSS 20.0 software package (SPSS Inc., Chicago, IL, USA) was used for data analysis. Quantitative data were expressed as the mean ± standard deviation. Statistical comparisons between groups were performed using the Student's *t*-test and one-way analysis of variance with the post test, when appropriate. $P<0.05$ was considered statistically significant.

Results

Cell morphological changes under acute hypoxia

Under normoxic conditions, cells retained their typical

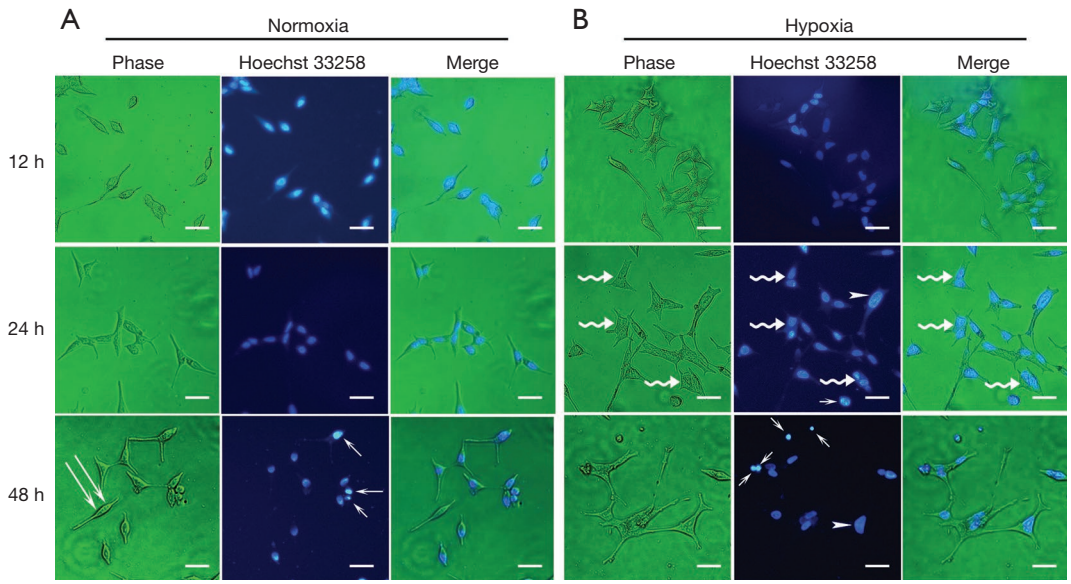

Figure 1 Representative images of phase-contrast photomicrographs and nuclei stained with Hoechst 33258 (bar =20 μm). Phase-contrast photomicrographs showed spike-like cells (double arrow) at 48 hours under normoxia (A). Hoechst 33258 staining of apoptotic cells (arrow), cell shrinkage, and condensed nuclei could be observed under both normoxia (A) and acute hypoxia (B). Acute hypoxia also led to nuclear aggregation (wave arrow, B) and enlarged nuclei (arrowhead).

spindle-shaped morphology at 12 hours, as described by Bratland *et al.* (16). A subset of LNCaP cells had characteristic, elongated cell shapes at 48 hours, showing an isolated and fibroblastoid-like morphology (*Figure 1A*). While under acute hypoxia, the LNCaP cells tended to aggregate (*Figure 1B*), appearing with a polygonal and flattened shape. Nuclear morphological analysis with Hoechst 33258 staining showed that apoptotic cells could be observed under both normoxia as well as acute hypoxia and were characterized by chromatin condensation, nuclear fragmentation, and formation of apoptotic bodies (*Figure 1A,B*). Moreover, cell nuclei tended to aggregate under acute hypoxia (*Figure 1B*), as evidenced by a few enlarged nuclei at 24 and 48 hours after culture (*Figure 1B*).

Time-dependent decrease in cell viability under acute hypoxia

There was no significant difference regarding the inhibition rate of cell viability between LNCaP cells under normoxia and acute hypoxia at 12 hours (20.09%±4.63% *vs.* 28.25%±4.33%). The inhibition rates of LNCaP cells were 42.24%±4.72% and 78.34%±8.44% at 24 and 48 hours under acute hypoxia, which were significantly higher than those of LNCaP cells under normoxia (32.02%±3.65%, $P<0.05$; 35.12%±5.44%, $P<0.01$; respectively). The inhibition rates were markedly increased at 24 and 48 hours of culture in a time-dependent manner under acute hypoxia. These data indicated decreased cell viability of LNCaP cells under acute hypoxia (*Figure 2*).

Acute hypoxia inhibited cell migration ability

Under normoxia, cell migration appeared to be a time-dependent behavior; whereas acute hypoxia resulted in an early and transient cell migration with a narrowed wound area at 12 hours, a subsequently expanded area similar to the initial wound at 24 hours, and finally exhibited an enlarged area at 48 hours post-wound scratch (*Figure 3A*). The wound closure areas under normoxia were 9.02%±8.71%, 15.38%±7.99%, and 28.26%±10.24% at 12, 24, and 48 hours, respectively, compared with 2.72%±10.67%, 0.14%±11.08%, and –11.825%±7.00% in serum-deprived, acute hypoxic conditions, respectively. The area of the wound was 10% larger than that of the initial wound area at 48 hours under acute hypoxia (*Figure 3B*, $P<0.01$). These observations suggested that LNCaP cells had a decreased capacity for migration in the presence of acute hypoxia.

Rapid and increased ROS production under acute hypoxia

The MFI was relatively low at 12 hours under both normoxic and acute hypoxic conditions, and no significant differences were found. However, LNCaP cells produced significantly more ROS under acute hypoxia at 24 hours (32,492.00±10,344.55 AU) than that under acute hypoxia at 12 hours (11,300.66±3969.75 AU, P<0.01). The MFI rapidly reached a peak at 24 hours under acute hypoxia, compared with that under normoxic conditions at 24 hours (32,492.00±10,344.55 *vs.*11,899.11±889.96 AU, P<0.01). The MFI level under acute hypoxia slightly decreased at 48 hours (25,513.22±4322.51 AU), remaining at a relatively high level, compared with that under hypoxic conditions at 24 hours (*Figure 4*).

ROS distributed heterogeneously among cells

To distinguish the distribution of DCF among cells, the iMFI within individual cells was analyzed. LNCaP cells under both normoxia and acute hypoxia exhibited two types of characteristic apoptotic morphologies, enlarged round cells and shrunken cells, with different fluorescence intensities. The former cellular morphology was enlarged and round with chromatin condensation; whereas the latter cellular morphology represented cytoplasm shrinkage, nuclear condensation, and apoptotic body formation. DCF

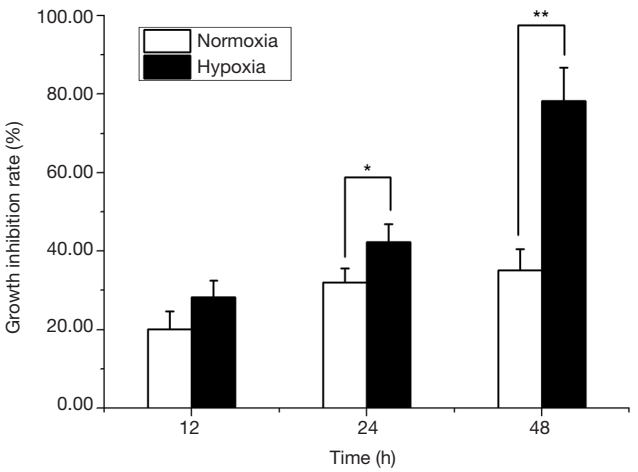

Figure 2 Inhibition rates of LNCaP cells treated with acute hypoxia using CCK-8 assay. The growth inhibition rate was obviously increased under acute hypoxia at 24 and 48 hours compared with that under normoxia (*P<0.05; **P<0.01).

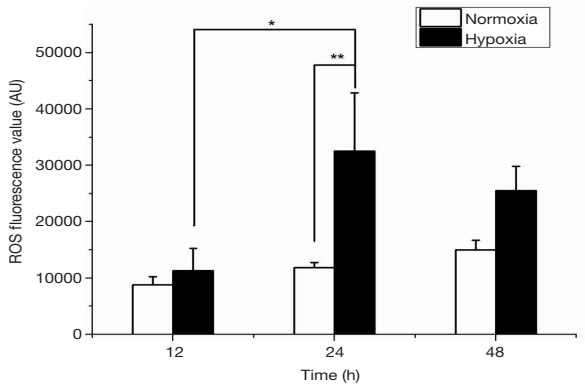

Figure 4 ROS generation in LNCaP cells exposed to acute hypoxia using the fluorescent probe DCFH-DA. Intracellular ROS production was determined by DCF fluorescence. The results were expressed as the MFI and were given as the mean ± standard deviation for three experiments (*P<0.05; **P<0.01). ROS, reactive oxygen species; DCFH-DA, 2',7'-dichlorofluoresceindiacetate; DCF, Dichlorofluorescein; MFI, mean fluorescence intensity.

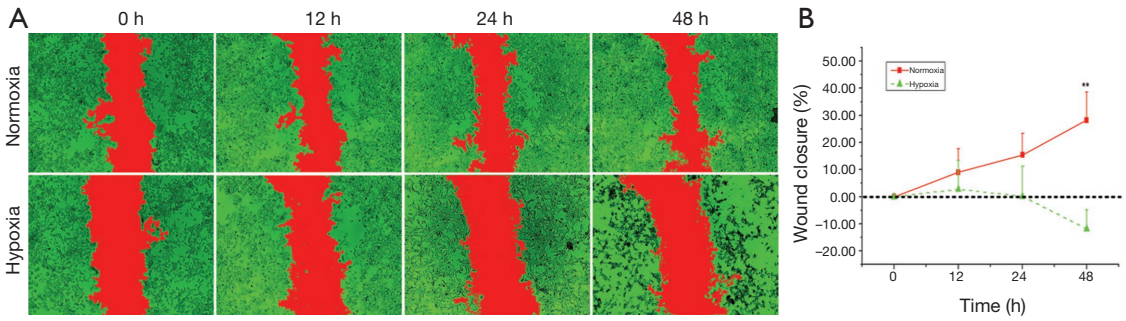

Figure 3 Wound healing assay (magnification, 40×). (A) LNCaP cells exhibited time-dependent cell migration under normoxia but a decreased capacity of cell migration in the presence of acute hypoxia. The red region denoted the scratch wound area over time; (B) quantitative measurement of cell migration. *P<0.05 *vs.* LNCaP cells under normoxia at 48 hours.

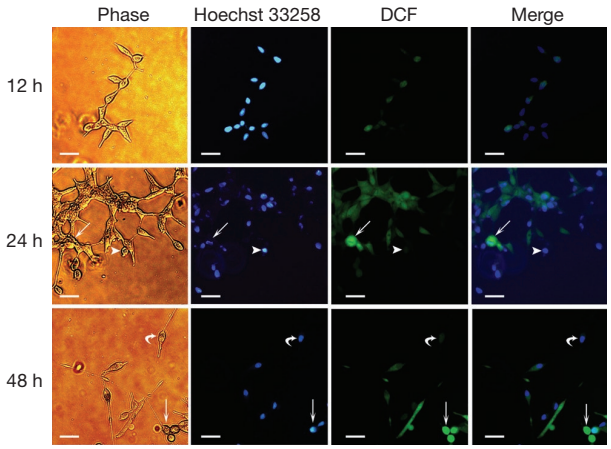

Figure 5 Distribution of DCF among cells under normoxia (bar =20 μm). The enlarged round cells demonstrated a strong green fluorescence (arrow). The iMFI of spindle-shaped cells (curved arrow) and shrunken cells with the formation of apoptotic bodies were weak (arrowhead). DCF, Dichlorofluorescein; iMFI, integrated MFI.

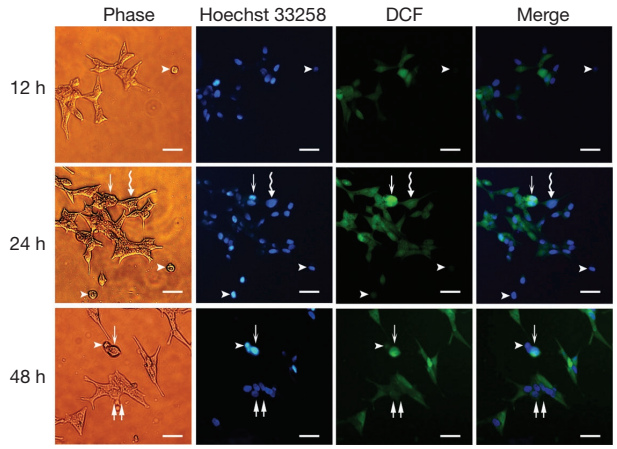

Figure 6 Distribution of Dichlorofluorescein (DCF) among cells under acute hypoxia (bar =20 μm). The iMFI of multicellular nucleus-aggregated cells (double arrow) and nucleus-enlarged cells (wave arrow) were moderate. Again, the fluorescence of enlarged round cells were strong (arrow), and the shrunken cells appeared extremely faint (arrowhead). DCF, Dichlorofluorescein; iMFI, integrated MFI.

in the enlarged round cells was stained much brighter than that of in the shrunken cells. For the LNCaP cells under normoxic conditions, the iMFI in the enlarged round cells at 24 hours was 20.48-fold higher than that of LNCaP cells at 12 hours, and 45.93-fold higher than that of the shrunken cells (*Figure 5*). For the LNCaP cells under acute hypoxia, the iMFI in the enlarged round cells at 24 hours was 31.54-fold higher than that of LNCaP cells at 12 hours, and 67.84-fold higher than that of the shrunken cells (*Figure 6*). Moreover, the iMFI in spindle-shaped morphological cells under normoxia at 48 hours was weak, which was 2.03-fold higher than that of LNCaP cells at 12 hours under normoxic conditions. The iMFI in aggregated cells under acute hypoxia at 48 hours was moderate, which was 13.38-fold higher than that of LNCaP cells at 12 hours under normoxic conditions (*Figure 6*). These results suggested that ROS was generated mainly in round apoptotic cells.

Percentages of apoptotic cells under acute hypoxia

The percentages of early apoptotic cells between LNCaP cells under normoxia and acute hypoxia at 12 hours showed no significant difference. The percentages of early apoptotic cells under acute hypoxia at 24 and 48 hours were 15.32%±2.34% and 24.11%±4.70%, respectively (*Figure 7A*), which were significantly greater than those under normoxia at the same time points (24 hours: 4.31%±0.92%, P<0.01; 48 hours: 6.22%±1.12%, P<0.01, *Figure 7B*). The percentages of late apoptotic cells at 12, 24, and 48 hours under acute hypoxia were 15.84%±2.81%, 26.81%±5.52%, and 46.42%±8.43%, respectively, showing a significant increase at 48 hours compared with that under normoxia (48 hours: 22.94%±4.14%, P<0.05, *Figure 7C*). These results indicated that acute hypoxia exacerbated cellular apoptosis in LNCaP cells in a time-dependent manner.

Collapse in ΔΨm under acute hypoxia

Membrane depolarization was found in the lower right quadrant of flow cytometry graphs, corresponding to the formation of JC-1 monomers and green fluorescence. As shown in *Figure 8A*, the loss of ΔΨm was observed in a time-dependent manner under both normoxia and acute hypoxia. The percentage of cells with JC-1 green fluorescence was not significantly altered under acute hypoxia at 12 hours (7.22%±1.46%), compared with that under normoxia (4.90%±1.22%, *Figure 8B,C*). However, significant increases in the percentage of LNCaP cells with JC-1 green fluorescence were observed under acute hypoxia at 24 hours (27.91%±5.34%) and 48 hours (36.62%±6.01%), 2.63-fold

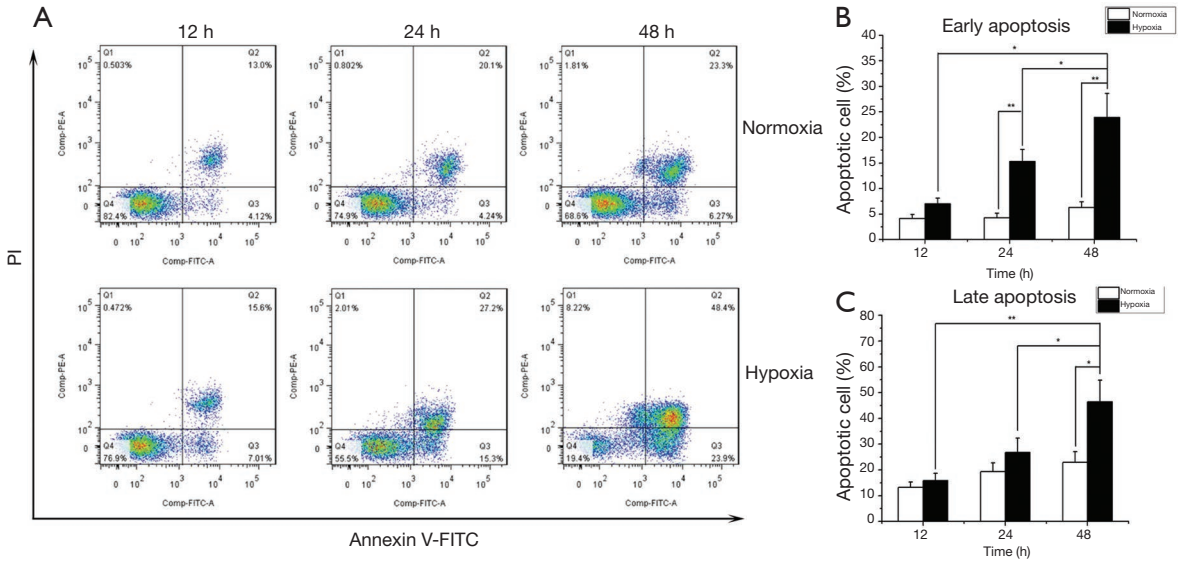

Figure 7 Time-dependent effect of acute hypoxia on LNCaP cell apoptosis. The data showed a time-dependent increase in the number of early apoptotic LNCaP cells (quadrant 3, annexin V^+/PI^-) and late apoptotic LNCaP cells (quadrant 2, annexin V^+/PI^+) under acute hypoxia, comparing to those under normoxia (A). Histograms showed an increased number of early apoptotic cells (B) and late apoptotic cells (C) under acute hypoxia (*P<0.05, **P<0.01).

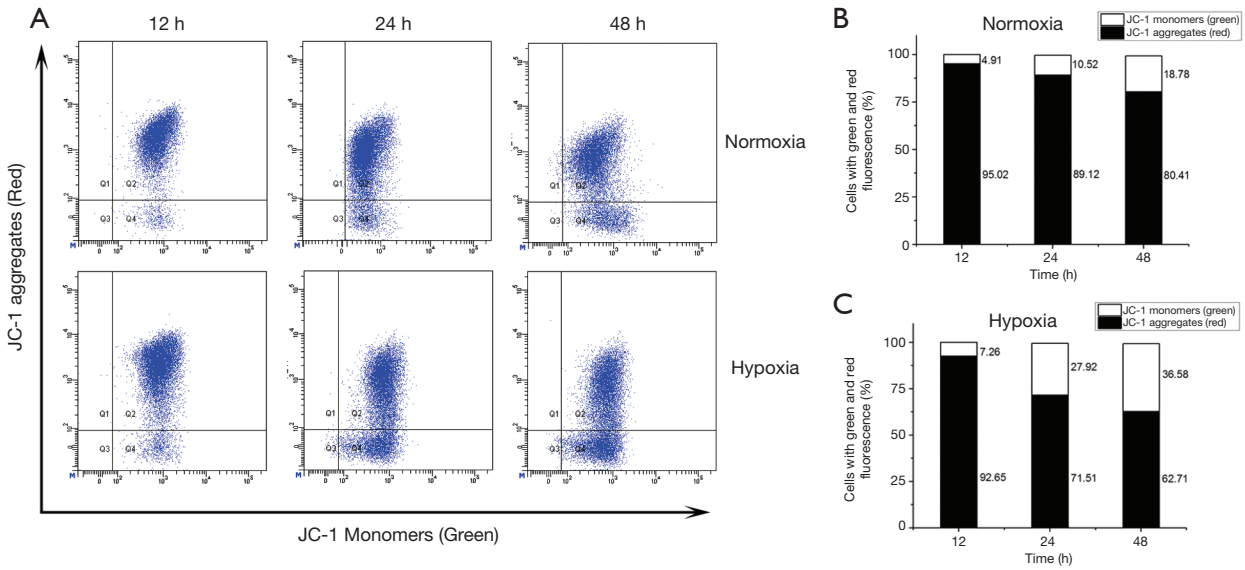

Figure 8 Effects of acute hypoxia on the mitochondrial membrane potential (ΔΨm) of LNCaP cells with JC-1 staining. FACS patterns of LNCaP cells labeled with JC-1 under normoxia or acute hypoxia were shown. Cells with polarized mitochondria (red fluorescence) were found in the upper right quadrant of the plots, and membrane depolarization (green fluorescence) were observed in the lower right quadrant (A). Quantification of FACS analysis under normoxia (B) and acute hypoxia (C).

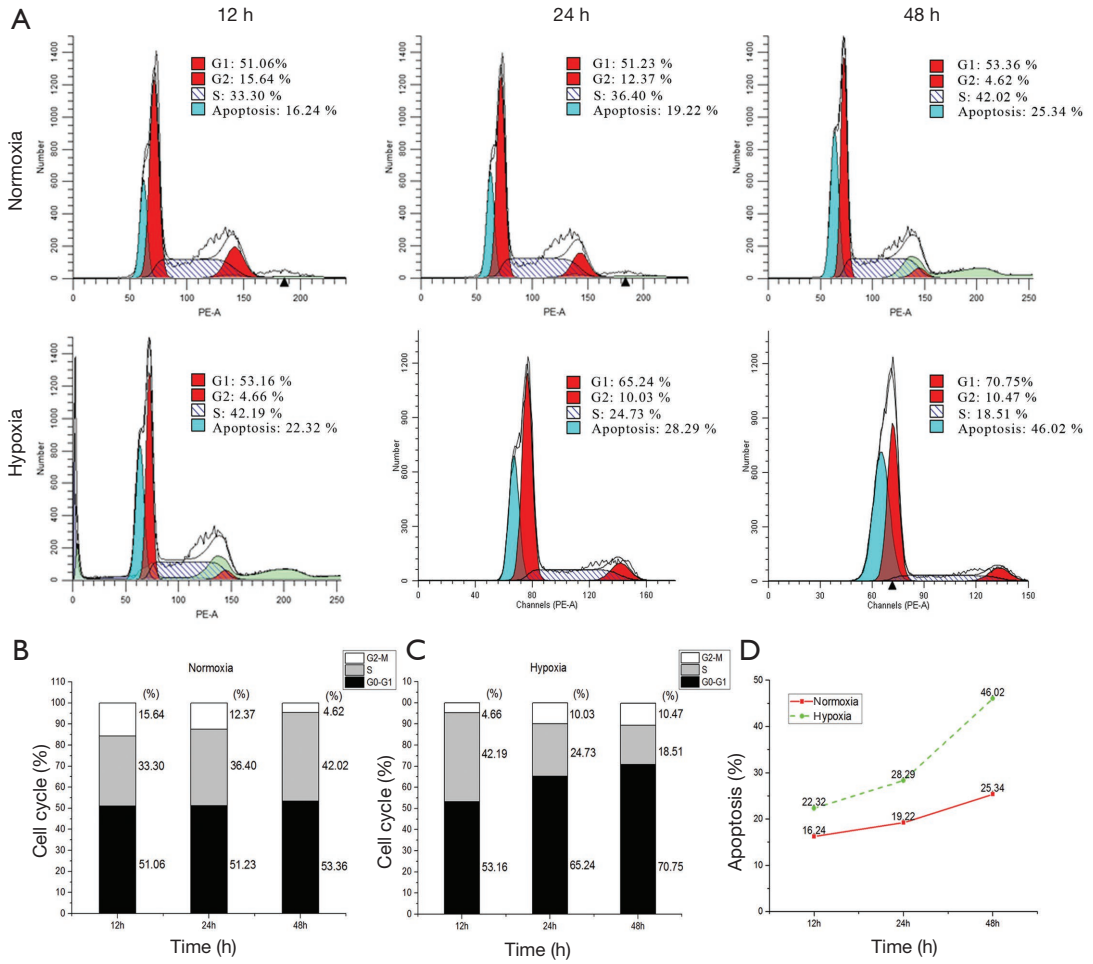

Figure 9 Representative images reflecting that acute hypoxia blocked cell cycle progression and exacerbates apoptosis in LNCaP cells. The influence of acute hypoxia on the cell cycle and apoptosis were assessed by flow cytometry (A); acute hypoxia induced an increase of LNCaP cells at the G0/G1 phases (B) and a decrease of LNCaP cells at the S phase (C); acute hypoxia led to a further increase in the apoptosis rate (D).

and 2-fold higher than those under normoxia at 24 hours (10.61%±2.41%, P<0.05) and 48 hours (18.21%±3.92%, P<0.05), respectively (*Figure 8B,C*). These data revealed acute hypoxia impaired ΔΨm in LNCaP cells.

Acute hypoxia increased the percentage of LNCaP cells in G0/G1 phases and reduced in S phases

As shown in *Figure 9A*, the LNCaP cell populations in the G0/G1 phases were not different when cultured under normoxia and acute hypoxia at 12 hours (51.04%±4.11% *vs.* 53.06%±3.71%, respectively). In contrast, the LNCaP cell populations in the G0/G1 phases under acute hypoxia were significantly higher than those under normoxia at 24 hours (65.24%±5.80% *vs.* 51.23%±4.00%, P<0.05); simultaneously, they were significantly reduced in the S phase (36.40%±4.09% *vs.* 24.73%±2.21%, P<0.05). Similar results were obtained when LNCaP cells were cultured for 48 hours. The LNCaP cell populations in the G0/G1 phases under acute hypoxia were significantly increased compared to those of LNCaP cells under normoxia (70.75%±9.39% *vs.* 53.36%±6.85%, P<0.01); simultaneously, they were significantly reduced in the S phase (42.02%±6.85% *vs.* 18.51%±2.39%, P<0.01, *Figure 9B,C*). Thus, once again, acute hypoxia was found to induce apoptosis in a time-dependent manner (*Figure 9D*). These results suggested that acute hypoxia induced G0/G1 arrest in LNCaP cells in a time-dependent manner, which is relevant to cell apoptosis.

Discussion

Human prostate cancer is a complex heterogeneous disorder in response to anticancer therapies. The disease becomes resistant to anti-androgen therapy when it transits from androgen-dependent to androgen-independent growth (16). Promising new approaches in the treatment of prostate cancer, such as targeted anticancer agents, have been under investigation. Animal models are essential for translation of research findings into new drug applications. The LNCaP animal model is believed to be appropriate because it mimics the pathophysiological process of prostate cancer. However, the take rate of LNCaP subcutaneous xenografts in nude mice is relatively low (17). Recent studies provide evidence that implanting cells at subcutaneous sites of immunodeficient mice may be a microenvironment with a poor blood supply and acute hypoxia (10). LNCaP cells have a more obvious preference for oxygen in comparison with PC3 and DU145 cells, which may be one of the causes for the low take rate achieved in mice. In this study, an acute-hypoxic LNCaP cell model was established to explore the impact of acute hypoxia on tumorigenic properties and the level of serum-deprived LNCaP apoptosis in response to a harsh microenvironment.

Our experiments confirmed morphological alterations of serum-deprived LNCaP cells in response to normoxic and acute hypoxic environments. We described a subset of serum-deprived LNCaP cells that exhibited an elongated and fibroblastoid-like shape under normoxia. These results indicated the involvement of LNCaP cells in the development of long-branched neuritic-like processes, which is a typical feature associated with epithelial-mesenchymal transition (18). The morphological changes ensure that the cells are better able to survive in a normoxic environment and even increase their potential aggressiveness. However, serum-deprived LNCaP cells tended to aggregate in response to acute hypoxia and formed multicellular aggregates, suggesting that LNCaP cells might lose their capacity to adhere to the extracellular matrix and thus are prone to cell apoptosis (19). These results demonstrated that acute hypoxia might increase the tendency for LNCaP cell apoptosis, in line with their morphological alterations.

Cell shape changes in response to different stimuli may impact cell motility and migration. Wound healing assay showed that LNCaP cells under normoxia moved faster than LNCaP cells under acute hypoxia. The fibroblastoid-like shape in a number of LNCaP cells might facilitate cell migration. Cell elongation contributes to cell migration from wound edges towards the wound center (20). However, serum-deprived LNCaP cells under acute hypoxia led to cell aggregation, resulting in failure of cell migration (21).

It is well established that an acute hypoxic microenvironment can induce ROS production. DCFH-DA can pass through cell membranes and is cleaved by intracellular esterases to produce DCF, which is trapped within the cells. An increased intensity of intracellular fluorescence is indicative of an increased level of generated ROS (22). Our study demonstrated that the MFI of LNCaP cells under acute hypoxia was significantly higher and earlier than that of cells under normoxia. Aside from the effect of acute hypoxia on ROS production in these cells, we also explored the variations of cellular iMFI in individual LNCaP cells. We observed that the ROS production was heterogeneously distributed among cells. Those round cells prone to detach had a significantly stronger diffusion of DCF fluorescence. The DCF-induced fluorescence is assumed to originate from a damaged mitochondrial intermembranous space, relocation of traces of low-mass labile iron compounds, and cytochrome c (23). Thus, a high intensity of intracellular fluorescence is associated with cellular apoptosis. Importantly, acute hypoxia is a crucial factor that induces early mitochondrial swelling in those round cells, which is considered as the first sign of cell damage (24). Unlike the enlarged, round apoptotic cells that exhibit a strong fluorescence signal, apoptotic cells with a shrunken cytoplasm and condensed nuclei exhibit a faint fluorescence signal, revealing that by themselves they are unable to oxidize H2DCF, given that mitochondria are within the cytoplasm (23). Interestingly, fibroblastoid-like cells under normoxia emitted a weak fluorescence. These findings indicate that these cells are flexible to maintain the integrity of the mitochondrial membrane, making themselves adapt to the corresponding normoxic conditions.

Since acute hypoxia can lead to an increase of ROS production and a decrease of cell viability, ultimately resulting in apoptosis, we further examined apoptotic LNCaP cells under acute hypoxia. An abnormal nuclear morphology of LNCaP cells stained with Hoechst 33258 was observed under both normoxia and acute hypoxia, indicating that LNCaP cells were affected by serum deprivation. Accumulating evidence has implicated that acute hypoxia has the potential to kill the affected tumor cells (25). In order to identify apoptotic cells quantitatively, annexin V/PI flow cytometry was used to measure the percentages of early and late apoptotic cells. The results

showed that the percentages of both early and late apoptotic LNCaP cells increased under acute hypoxia, in comparison with LNCaP cells under normoxia.

Hypoxia induces ROS production and loss of ΔΨm (26), which increase susceptibility to apoptosis. We found that the percentage of LNCaP cells with a depolarized membrane potential at 24 hours was nearly 3-fold higher than that of LNCaP cells under normoxia. Additionally, an increased ROS production can trigger cell cycle arrest (27). Our experiments confirmed that serum-deprived LNCaP cells under acute hypoxia underwent cell cycle arrest at the G0/G1 phases, which was consistent with the findings by Yamasaki *et al.* (28).

Several limitations were noted in the present study. One limitation was the selection of prostate cell lines; only androgen-dependent LNCaP cells with poorly tumorigenic ability were involved. The androgen-independent DU145 and PC-3 cells with relatively higher tumor formation rate were not considered in the present study. However, in view of the intrinsic heterogeneity of prostate cancer tumors, further study with the comparison of different prostate cancer cell lines may be required. Another limitation was the absence of experiments *in vivo*. Establishment of an ideal *in vivo* experimental model for mimicking the subcutaneous acute hypoxic microenvironment in mice is needed in future study.

Conclusions

In summary, our study determined that acute hypoxia led to morphological alterations, decreased cell viability and migration, and increased ROS production in serum-deprived LNCaP cells. Increased ROS production induced cellular apoptosis, cell cycle arrest, and collapse of the ΔΨm, thus drastically affecting the survival of LNCaP cells. These findings add to our existing knowledge of the detrimental effects of acute hypoxia on LNCaP cells and are valuable to better understand the mechanisms involved in the acute hypoxia-induced apoptosis of LNCaP cells.

Acknowledgments

Funding: This research was supported by the Science and Technology Commission of Shanghai Municipality Foundation (No. 14140901802) and National Natural Science Foundation of China (No. 81671708).

Footnote

Conflicts of Interest: All authors have completed the ICMJE uniform disclosure form (available at http://dx.doi.org/10.21037/tcr.2017.10.13). The authors have no conflicts of interest to declare.

Ethical Statement: The authors are accountable for all aspects of the work in ensuring that questions related to the accuracy or integrity of any part of the work are appropriately investigated and resolved. The study was conducted in accordance with the Declaration of Helsinki (as revised in 2013). Institutional ethical approval and informed consent were waived.

References

1. Fowke JH, McLerran DF, Gupta PC, et al. Associations of Body Mass Index, Smoking, and Alcohol Consumption With Prostate Cancer Mortality in the Asia Cohort Consortium. Am J Epidemiol 2015;182:381-9.
2. Qi JL, Wang LJ, Zhou MG, et al. Disease burden of prostate cancer among men in China, from 1990 to 2013. Zhonghua Liu Xing Bing Xue Za Zhi 2016;37:778-82.
3. Bruce JY, Lang JM, McNeel DG, et al. Current Controversies in the Management of Biochemical Failure in Prostate Cancer. Clin Adv Hematol Oncol 2012;10:716-22.
4. Suzuki S, Naiki-Ito A, Kuno T, et al. Establishment of a syngeneic orthotopic model of prostate cancer in immunocompetent rats. J Toxicol Pathol 2015;28:21-6.
5. Grigoryev DN, Long BJ, Njar VC, et al. Pregnenolone stimulates LNCaP prostate cancer cell growth via the mutated androgen receptor. J Steroid Biochem Mol Biol 2000;75:1-10.
6. Graeser R, Chung DE, Esser N, et al. Synthesis and biological evaluation of an albumin-binding prodrug of doxorubicin that is cleaved by prostate-specific antigen

(PSA) in a PSA-positive orthotopic prostate carcinoma model (LNCaP). Int J Cancer 2008;122:1145-54.
7. Cunningham D, You Z. In vitro and in vivo model systems used in prostate cancer research. J Biol Methods 2015;2:1-28.
8. He L, Tian DA, Li PY, et al. Mouse models of liver cancer: Progress and recommendations. Oncotarget 2015;6:23306-22.
9. Varna M, Bertheau P, Legrès L. Tumor Microenvironment in Human Tumor Xenografted Mouse Models. J Anal Oncol 2014;3:159-66.
10. Ahmed SU, Zair M, Chen K, et al. Generation of subcutaneous and intrahepatic human hepatocellular carcinoma xenografts in immunodeficient mice. J Vis Exp 2013;(79):e50544.
11. Higgins LH, Withers HG, Garbens A, et al. Hypoxia and the metabolic phenotype of prostate cancer cells. Biochim Biophys Acta 2009;1787:1433-43.
12. Sermeus A, Genin M, Maincent A, et al. Hypoxia-induced modulation of apoptosis and BCL-2 family proteins in different cancer cell types. PLoS One 2012;7:e47519.
13. Baek JH, Jang JE, Kang CM, et al. Hypoxia-induced VEGF enhances tumor survivability via suppression of serum deprivation-induced apoptosis. Oncogene 2000;19:4621-31.
14. Bonavita F, Stefanelli C, Giordano E, et al. H9c2 cardiac myoblasts undergo apoptosis in a model of ischemia consisting of serum deprivation and hypoxia: inhibition by PMA. FEBS Lett 2003;536:85-91.
15. van der Meer AD, Vermeul K, Poot AA, et al. A microfluidic wound-healing assay for quantifying endothelial cell migration. Am J Physiol Heart Circ Physiol 2010;298:H719-25.
16. Bratland A, Boender PJ, Hoifodt HK, et al. Osteoblast-induced EGFR/ERBB2 signaling in androgen-sensitive prostate carcinoma cells characterized by multiplex kinase activity profiling. Clin Exp Metastasis 2009;26:485-96.
17. Zou M, Jiao J, Zou Q, et al. Multiple metastases in a novel LNCaP model of human prostate cancer. Oncol Rep 2013;30:615-22.
18. Chen H, Shen A, Zhang Y, et al. Pien Tze Huang inhibits hypoxia-induced epithelial-mesenchymal transition in human colon carcinoma cells through suppression of the HIF-1 pathway. Exp Ther Med 2014;7:1237-42.
19. Morimoto-Kamata R, Mizoguchi S, Ichisugi T, et al. Cathepsin G induces cell aggregation of human breast cancer MCF-7 cells via a 2-step mechanism: catalytic site-independent binding to the cell surface and enzymatic activity-dependent induction of the cell aggregation. Mediators Inflamm 2012;2012:456462.
20. Mousavi SJ, Hamdy Doweidar M. Three-Dimensional Numerical Model of Cell Morphology during Migration in Multi-Signaling Substrates. Plos One 2015;10:e0122094.
21. Pocha SM, Montell DJ. Cellular and Molecular Mechanisms of Single and Collective Cell Migrations in Drosophila: Themes and Variations. Annu Rev Genet 2014;48:295-318.
22. Rahman MA, Hussain A. Anticancer activity and apoptosis inducing effect of methanolic extract of Cordia dichotoma against human cancer cell line. Bangladesh J Pharmacol 2015;10:27-34.
23. Karlsson M, Kurz T, Brunk UT, et al. What does the commonly used DCF test for oxidative stress really show? Biochem J 2010;428:183-90.
24. Niquet J, Baldwin RA, Allen SG, et al. Hypoxic neuronal necrosis: protein synthesis-independent activation of a cell death program. Proc Natl Acad Sci U S A 2003;100:2825-30.
25. Hernansanz-Agustín P, Izquierdo-Álvarez A, Sánchez-Gómez FJ, et al. Acute hypoxia produces a superoxide burst in cells. Free Radic Biol Med 2014;71:146-56.
26. Srinivasan S, Koenigstein A, Joseph J, et al. Role of mitochondrial reactive oxygen species in osteoclast differentiation. Ann N Y Acad Sci 2010;1192:245-52.
27. Liou GY, Storz P. Reactive oxygen species in cancer. Free Radic Res 2010;44:479-96.
28. Yamasaki M, Nomura T, Sato F, et al. Chronic hypoxia induces androgen-independent and invasive behavior in LNCaP human prostate cancer cells. Urol Oncol 2013;31:1124-31.

Cite this article as: Liu W, Zhu Y, Jiang J, Jiang X, Chen Y. Acute hypoxia induces apoptosis in serum-deprived prostate cancer LNCaP cells. Transl Cancer Res 2017;6(6):1283-1293. doi: 10.21037/tcr.2017.10.13

